International Journal of Environmental Sciences
ISSN: 2229-7359
Vol. 11 No. 12s,2025
https://theaspd.com/index.php

Study the nuclear structure for some nuclei in the island of inversion region using the shell model and Hartree-Fock calculations

Luay F. Sultan[1], Ali A. Alzubadi[2]
Department of Physics-College of Science-University of Baghdad

Abstract
The study of neutron-rich nuclei around and in Nuclear Island of Inversion region (N ≈ 20) offers critical insights into shell evolution, the erosion of traditional magic numbers, and the emergence of intruder configurations. In this work, we investigate the static and dynamic nuclear structure properties of Al, Na, and F isotopes through a combination of large-scale shell model calculations. Shell model calculations were performed in the sd-shell model space using the USDA, USDB, and USDC effective interactions, and in a truncated no-core spsdpf model space using the FSU interaction, determined in this study. Key observables such as excitation energies, B(E2) transition probabilities, binding energies, two-neutron separation energies, shell evolution, and longitudinal C2 electroexcitation form factors were systematically analyzed. The results demonstrate that while traditional sd-shell interactions are inadequate for capturing the enhanced collectivity and cross-shell excitations characteristic of the island of inversion, the FSU interaction provide a much-improved description of the evolving shell structure.
Key words: *Shell model, Neutron-rich nuclei, Island of inversion, intruder state*

1. INTRODUCTION

The exploration of nuclear structure remains a fundamental topic in nuclear physics, where the shell model stands out as one of the most effective theoretical approaches. This model provides insight into the behavior of nucleons (protons and neutrons) within the nucleus by assuming their arrangement in distinct energy levels, much like electrons in atomic orbitals. Over recent years, significant attention has shifted towards the study of neutron-rich nuclei those containing a greater number of neutrons than protons because they exhibit unique characteristics that challenge conventional models and contribute to the understanding of nuclear interactions [1,2]. One intriguing discovery in this area is the "Island of Inversion" (IOI), a region in the nuclear landscape where the expected shell structure is disrupted due to unusual nucleon interactions. This phenomenon results in the emergence of non-standard configurations and deformed states that deviate from traditional shell model predictions, highlighting the complexity of nuclear forces in neutron-rich environments [3]. To capture the intricate nature of these structures, the configuration mixing (CM) approach becomes essential. This method accounts for the coexistence of multiple configurations within nuclei by considering interactions among different nucleonic arrangements, which leads to a more accurate depiction of nuclear states [4]. In this context, investigating the nuclei near the IOI region using both the *sd shell* and *no-core model spaces* (NCSM) provides valuable insights. Two-body effective interactions in nuclear physics are a conceptual framework that simplifies the study of nuclear interactions by focusing on pairwise nucleon interactions within nuclei. This approach facilitates a more manageable analysis of nuclear phenomena while preserving the essential features of the complex many-body nuclear system [5]. The sd shell model is one of the key models in nuclear physics for studying the structural properties of nuclei with mass numbers ranging between 16 and 40. This model relies on a set of fundamental shell orbitals, including $1d_{5/2}$, $2s_{1/2}$, and $1d_{3/2}$, which play a crucial role in describing the spatial distribution and probability of nucleons within the nucleus. The study of nuclei in the sd shell region requires specialized effective interactions that account for nucleon-nucleon forces in a precise and comprehensive manner. Among the most prominent interactions used in this model are USDA, USDB [6], and USDC [7]. The USDA interaction excels at improving predictions related to binding energies for lighter nuclei, demonstrating its effectiveness in describing these nuclei in terms of

nuclear binding and relative stability. On the other hand, the USDB interaction offers superior accuracy when studying neutron-rich nuclei, as it considers dynamic changes resulting from high neutron density. Meanwhile, the USDC interaction stands out for its efficiency in addressing nuclei that exhibit strong configuration mixing and the presence of intruder states. These states arise due to the interaction between energy levels beyond conventional shell model expectations, necessitating advanced interactions that account for such complex effects to ensure a more accurate description of these nuclear systems. In contrast, the *no-core model space* removes the assumption of an inert core, treating all nucleons as active participants. This allows precise modeling of exotic nuclei. Within this approach [7], the Florida State University (FSU) [8] interaction plays a pivotal role by incorporating tensor forces and configuration mixing, which significantly enhance predictions for nuclear energy levels and transition probabilities. Additionally, the Skyrme-Hartree-Fock (SHF) method offers a powerful framework for studying nuclear structure by employing effective Skyrme potentials to represent nucleon interactions. This method supports precise calculations of nuclear properties such as deformation, energy levels, and density distributions, which are essential for understanding neutron-rich systems [9].

Several previous studies underscore the importance of these methods in the investigation of neutron-rich nuclei. The low-energy level structure of the exotic Na isotopes ^{28,29}Na has been investigated through β-delayed γ spectroscopy by Tripathi et al. [10] which presents the first detailed spectroscopy of 28 ,29Na, clearly demonstrates that such a transition in the Na isotopes occurs between ^{28}Na (N = 17) and ^{29}Na (N = 18), supporting the smaller N = 20 shell gap in neutron rich sd shell nuclei. Doornenbal et al. [11] investigated the structure of the neutron-rich sodium isotopes ^{31,32,33}Na by means of in-beam γ-ray spectroscopy following one-neutron knockout and inelastic scattering of radioactive beams provided by the RIKEN Radioactive Ion Beam Factory.

The primary objective of the present research is to investigate the static and dynamic properties of F, Na, and Al isotopes, within the IOI region. Key nuclear properties such as excitation energy, binding energy, reduced transition probability, separation energy, shell evolution, and inelastic longitudinal C2 form factors will be analyzed. The study will further assess the impact of using different shell model spaces and two-body effective interactions, including USDA, USDB, USDC, and FSU, as well as employing SHF as a single-particle potential framework.

2. THEORY

The many particles reduced matrix element of the electric multipole transition operator for an A-particle model space wave function of multipolarity λ is expressed as the sum of the product over the one-body density matrix (OBDM) elements times reduced Single-particle matrix elements, and is given by [12]

$$\langle f \parallel \hat{T}^{\lambda} \parallel i\rangle = \langle n\omega_f J_f \parallel \hat{T}^{\lambda} \parallel n\omega_i J_i\rangle = \sum_{k\alpha k\beta} OBDM\left(f, i, k_\alpha, k_\beta, \lambda\right)\langle k_\alpha \parallel \hat{T}^{\lambda} \parallel k_\beta\rangle \quad (1)$$

where *ki, kf* are single –particle state for initial and final model space state (*nwiJi*) and (*nwfJf*) respectively. Also, ω indicates indices to differentiate between various states having the same J values. Giving rise to formalism of OBDM in the proton-neutron as follows [12].

$$OBDM\left(f, i, k_{\alpha,t_z}, k_{\beta,t_z}, \lambda\right) = \frac{\langle n\omega_f J_f \parallel \left[a^{+}_{k_{\alpha,t_z}} \otimes \tilde{a}_{k_{\beta,t_z}}\right]^{\lambda} \parallel n\omega_i J_i\rangle}{\sqrt{2\lambda+1}} \quad (2)$$

The Hamiltonian is written as a sum of three terms [13]

$$\hat{H} = \hat{H}_{nn} + \hat{H}_{pp} + \hat{H}_{pn} \quad (3)$$

the second quantized form for H_{pn} is [13]

$$\hat{H}_{pn} = \sum_{pnp'n'j_\circ} \left\{ \left[a_p^+ a_n^+ \right]^{j_o} \otimes \left[\tilde{a}_{p'} \tilde{a}_{n'} \right]^{j_o} \right\}^{(0)} \quad (4)$$

we can recouple the operators to [13]

$$\left\{ \left[a_p^+ a_n^+ \right]^{j_o} \otimes \left[\tilde{a}_{p'} \tilde{a}_{n'} \right]^{j_o} \right\}^{(0)} = -\sum_\lambda \sqrt{(2\lambda+1)(2j_\circ+1)}(-1)^{j_n + j_{p'} - \lambda - j_o} \times \begin{Bmatrix} j_p & j_n & j_o \\ j_{n'} & j_{p'} & \lambda \end{Bmatrix} \times \left\{ \left[a_p^+ \tilde{a}_{p'} \right]^\lambda \otimes \left[a_n^+ \tilde{a}_{n'} \right]^\lambda \right\}^{(0)} \quad (5)$$

where, for example, p stands for the single-particle wave function (n_p, l_p, j_p). H_{pn} can thus be written in the particle-hole form [13]

$$H_{pn} = \sum_{pp'nn'\lambda} F_\lambda(pp'nn') \left\{ \left[a_p^+ \tilde{a}_{p'} \right]^\lambda \otimes \left[a_p^+ \tilde{a}_{n'} \right]^\lambda \right\}^{(0)} \quad (6)$$

Where

$$F_\lambda(pp'nn') = -\sum_{j_o} \sqrt{(2\lambda+1)(2J+1)}(-1)^{n+p'-\lambda-J_o} \times \begin{Bmatrix} p & n & J_o \\ n' & p' & \lambda \end{Bmatrix} \quad (7)$$

The Skyrme effective interaction was developed from the postulation that the energy functional could be expressed in terms of a zero-range expansion, leading to a simple derivation of the Hartree-Fock (HF) equations. The two-body terms are written as a shortrange expansion in the form [14-17].

$$V_{Skyrme}(r_1, r_2) = t_0\left(1 + x_0 \hat{P}_\sigma\right)\delta_{12} + \frac{t_1}{2}\left(1 + x_1 \hat{P}_\sigma\right)\left[\vec{k}'^2 \delta_{12} + \delta_{12}\vec{k}^2\right] + t_2\left(1 + x_2 \hat{P}_\sigma\right)\vec{k}'^2 \delta_{12} + \frac{t_3}{6}\left(1 + x_3 \hat{P}_\sigma\right)\rho\left(\frac{\vec{r}_1 \vec{r}_2}{2}\right)\delta_{12} + iW_0 \vec{k}' \delta_{12}\left(\vec{\delta}_1 + \vec{\delta}_2\right) \times \vec{k} + \frac{t_e}{2}\left(\left[3\left(\vec{\delta}_1 . \vec{k}'\right)\left(\vec{\delta}_2 . \vec{k}'\right) - \left(\vec{\delta}_1 . \vec{\delta}_2\right)\vec{k}'^2\right]\delta_{12} + \delta_{12}\left[3\left(\vec{\delta}_1 . \vec{k}\right)\left(\vec{\delta}_2 . \vec{k}\right) - \left(\vec{\delta}_1 . \vec{\delta}_2\right)\vec{k}^2\right]\right) + t_0\left[3\left(\vec{\delta}_1 . \vec{k}\right)\delta_{12}\left(\vec{\delta}_2 . \vec{k}\right) - \left(\vec{\delta}_1 . \vec{\delta}_2\right)\vec{k}' \delta_{12}\vec{k}\right] \quad (8)$$

where $\delta_{12} = \delta(\vec{r_1} - \vec{r}_2))$ and k, k' are the relative momentum operators with k acting on the right, while k' is the operator acting on the left and are given by [18]:

$$\vec{k}' = -\frac{1}{2i}\left(\vec{\nabla}_1 - \vec{\nabla}_2\right), \vec{k} = \frac{1}{2i}\left(\vec{\nabla}_1 - \vec{\nabla}_2\right) \quad (9)$$

also, is the spin-exchange operator that are given as:

$$\hat{P}_\sigma = \frac{1}{2}\left(1 + \hat{\sigma}_1 . \hat{\sigma}_2\right) \quad (10)$$

where are the Pauli spin matrices. The Skyrme parameterizations; x_n, t_n, t_o, t_e, α and W_0 are the free parameters, that are must be fitted to nuclear structure experimental data. Each term creates both time-even and time-odd densities in the HF equations [19].

The longitudinal electroexcitation form factor is related to the charge density distribution through the matrix elements of multipole operators $\hat{T}_J^L(q)$ [20].

$$\left|F_J^L(q)\right|^2 = \frac{4\pi}{Z^2(2J_i+1)}\left|\langle f \| \hat{T}_J^L(q) \| i \rangle\right|^2 |F_{cm}(q)|^2 \left|F_{fs}(q)\right|^2 \quad (11)$$

where Z is the proton number in the nucleus and $F_{cm}(q)$ is the center of mass correction, $F_{fs}(q)$ is the finite size correction.

The reduced electric transition probability in terms of the reduced many particle matrix elements of the electric transition operator is defined as [21]

$$B(EJ) = \frac{[(2J+1)!!]^2}{k^{2J}} \frac{\left|\langle J_f \| \hat{T}^{el} \| J_i \rangle\right|^2}{2J_i+1} \quad (12)$$

where k is the wave number. The reduced electric transition probability is in units of $e^2.fm^{2J}$.

3. RESULT AND DISCUSSIONS

The SHF single-particle potential, as well as the USDA, USDB, USDC, and FSU two-body effective interactions, have been used in the sd and no-core model spaces in this study. All theoretical computations were conducted using the NushellX@MSU shell model code [20], which was developed at Michigan State University. This code has been designed to perform large-scale shell model calculations, rendering it a widely employed tool for studying the behavior of nuclei in regions of interest, including the Nuclear Island of Inversion (NIOI) and the nuclear drip lines.

3.1. Low-laying excited state and excitation energy

Fig.1(a) presents the excitation energies for the transition to the low-lying 2^+ state in Al isotopes, compared with experimental data from Ref. [22]. The calculated results indicate that the expected inverse relationship between excitation energy and reduced transition probability Fig. 1(b) does not hold in or around the N=14 and 18 regions when using the *sd* model space. This deviation persists even after altering the two-body effective interactions between USDA, USDB, and USDC. While these interactions are generally reliable for typical *sd*-shell nuclei, they prove inadequate within the island of inversion. The primary reason for this limitation is the reduction of the shell gap and the emergence of intruder configurations. Specifically, the N=20 shell gap diminishes in neutron-rich nuclei, leading to significant structural changes that affect excitation energies and transition probabilities. This leads to significant mixing with intruder states from the *fp*-shell. Since these interactions do not account for excitations into the *fp*-shell, they are inadequate for accurately reproducing experimental trends. In the NIOI, the excitation energies of the 2^+ state ($E(2^+)$) are lower than expected due to strong quadrupole collectivity. Because *sd* interactions do not include cross-shell excitations, they tend to overestimate $E(2^+)$ and underestimate B(E2) values. The success of the truncated NCSM space with the FSU interaction in reproducing experimental data can be attributed to its ability to include cross-shell excitations and capture the underlying many-body correlations missing in traditional shell model calculations. Unlike the standard shell model, which confines nucleons within a single major shell, the NCSM allows for excitations into the *fp*-shell, effectively incorporating the intruder configurations that play a crucial role in the island of inversion. The FSU interaction is designed to have cross-shell interactions between the *sd*- and *fp*-shells in a manner that appropriately accounts for the quenching of the *N*=20 shell gap and enhanced collectivity in these nuclei.

International Journal of Environmental Sciences
ISSN: 2229-7359
Vol. 11 No. 12s,2025
https://theaspd.com/index.php

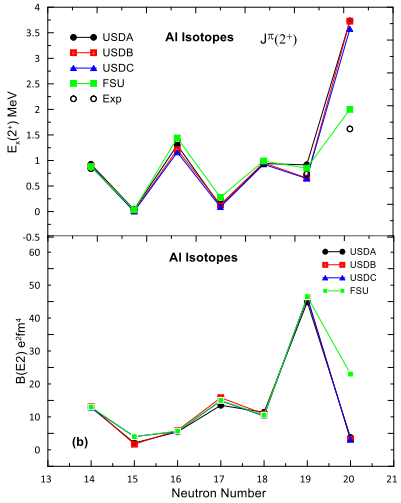

Fig. 1. Excitation energies (a) and B (E2; $0^+ \rightarrow 2^+$) values (b) for Al isotopes calculated using USDA, USDB, USDC, and FSU interactions compared with experimental data [22].

Fig. 2 illustrates the behavior of excitation energies E_x (2^+) and electric quadrupole transition probabilities B(E2;$0^+ \rightarrow 2^+$) for sodium isotopes, using various theoretical nuclear interactions (USDA, USDB, USDC, and FSU) compared to experimental data. The excitation energies shown in part (a) demonstrate good agreement with experiment, with a prominent peak at neutron number N=16 across all interactions. This indicates a shell closure that provides nuclear stability and makes excitation more difficult. In contrast, excitation energies decrease in other isotopes, indicating increased nuclear deformation and easier excitation. In Fig. 2 (b), the B(E2) values reflect the degree of collective nuclear deformation, showing high values at N=12N = 12 and very low values at N=16N = 16, consistent with a transition from a deformed nucleus to a more spherical one. However, what stands out is the behavior at N=20, where a significant increase in B(E2) is observed, especially in the FSU interaction, despite N=20 being a traditional magic number that typically implies a stable, spherical nuclear shape, at N=20, exhibit properties indicating shell closure breakdown and the emergence of intruder configurations, where neutrons occupy higher orbitals (such as $f_{7/2}$) in the ground state. This orbital mixing enhances collective effects and nuclear deformation, leading to low excitation energies and significantly increased transition probabilities, as seen in the FSU model. Therefore, the behavior observed at N=20 not only reflects differences among the models, but also signals a fundamental shift in the nuclear structure from regular shell-model behavior to strong collective deformation. It highlights the need for models that incorporate deformation and intruder effects to accurately describe the structure of light nuclei.

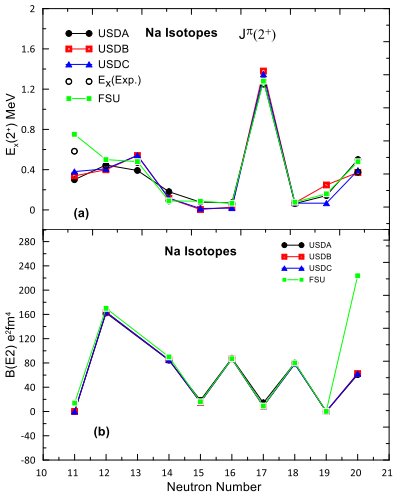

Fig. 2. Excitation energies (a) and B (E2; $0^+ \rightarrow 2^+$) values (b) for Na isotopes calculated using USDA, USDB, USDC, and FSU interactions compared with experimental data [22]

International Journal of Environmental Sciences
ISSN: 2229-7359
Vol. 11 No. 12s,2025
https://theaspd.com/index.php

The calculated values of F isotopes in Fig. 3 reveal that predictions made by USDA, USDB, and USDC interactions are in overall consensus and validate sd-shell energy stability. In this region, nuclei are moderately deformed and become increasingly spherical as a function of increasing neutron numbers. This is observed in the consistent decrease in B(E2) values as a hallmark of nuclear shape transition towards spherical. The very good agreement between these calculated predictions and experimental values validates that these interactions are trustworthy in predicting shell structures. An exception occurs at N = 18, where a decrease in excitation energy is a signature for the onset of neutron intruder orbital influence NIOI. These interactions do not fully explain this decrease and are consequently underestimating nuclear deformation effects. This discrepancy suggests that these interactions are not fully sufficient in accounting for intruder configuration effects on nuclear structure beyond the sd shell. In contrast, calculations with the FSU interaction agree with experiment data. This interaction reproduces the observed excitation energies and provides a better description of sd and pf shell interplay. This enhanced predictive capability is a consequence of the introduction of tensor force effects and intruder states that are very relevant in shell evolution in this regime. These results emphasize that nuclear structure modeling in neutron-rich isotopes should include higher-order interactions.

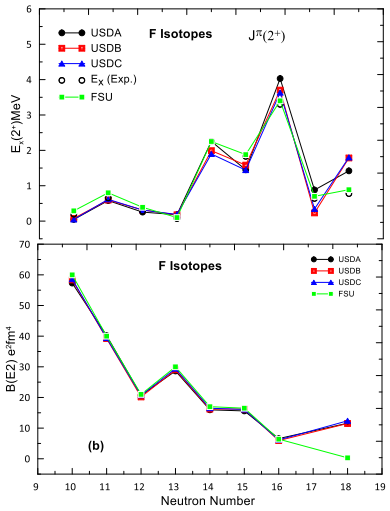

Fig.3. Excitation energies (a) and B (E2; $0^+ \rightarrow 2^+$) values (b) for F isotopes calculated using USDA, USDB, USDC, and FSU interactions compared with experimental data [22]

4.3.2. Nuclear binding energy and Separation energy

Fig. 4. shows the binding energy as a function of neutron number. There is a clear agreement between the calculated energy and the general pattern in the experimental data. It was observed that the binding energy curve of Al, Na, and F nuclei increases as the number of nucleons increases. A sharp increase in binding energy per nucleon occurs from beginning up to N=16, indicating the filling of energy levels or shells, resulting in increased stability. This is likely due to the filling of the p-shell, which becomes filled at N=16. A closed shell configuration at N=16 creates increased stability and higher binding energy per nucleon. A slight increase in binding energy per nucleon occurs from 16 to 21 after the p-shell is filled, possibly due to the gradual filling of the d-shell, which adds additional stability to the nuclei

International Journal of Environmental Sciences
ISSN: 2229-7359
Vol. 11 No. 12s,2025
https://theaspd.com/index.php

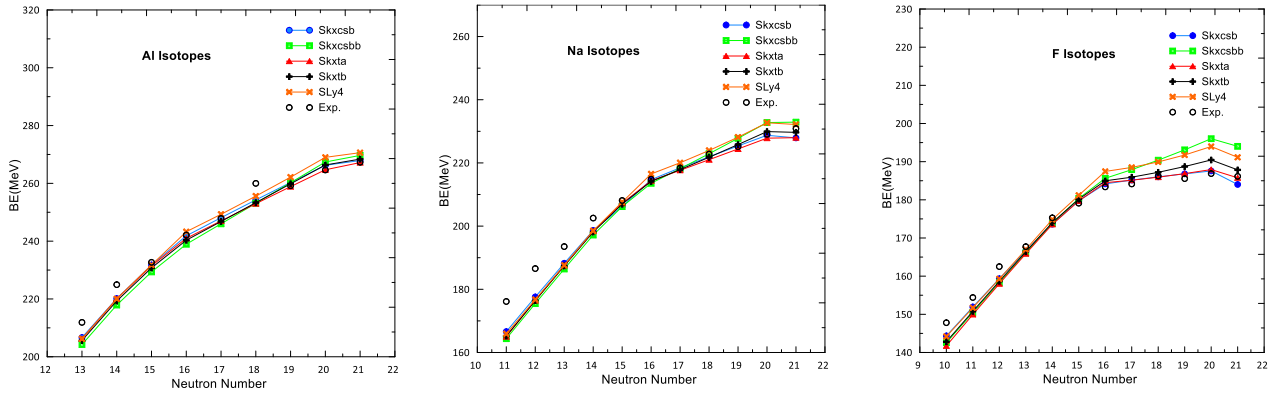

Fig. 4. Binding energies of Al (a), Na (b), and F (c) isotopes calculated using various Skyrme parameterizations within SHF and compared with experimental data [22].

Fig. 5. illustrates the relationship between the two-neutron separation energy and the number of neutrons for the isotopes Al, Na, and F. As the number of neutrons increases, the two-neutron separation energy decreases. We observe a gradual decrease from beginning up to N = 16 as a result of the increased neutron number, which consequently leads to nuclear stability. The sudden drop in neutron separation energy from N = 16 to N = 18. This sudden drop is due to the filling of a neutron shell (p shell), resulting in increased nuclear stability. The gradual decline continues, going from N = 18 to N = 21. At this point, the sharp decrease must continue because the sd shell will be filled, but on the contrary, the decrease is slight, and the reason for this is that we are approaching the island of inversion region and the appearance of the intruder state in configuration that leads to the disappearance of the magical properties at N = 20

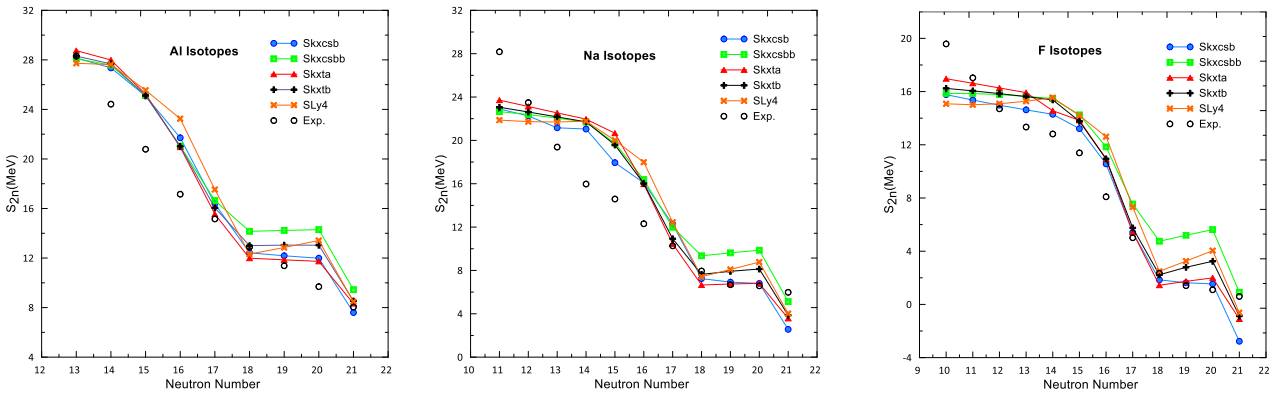

Fig. 5. Two-neutron separation energies (S_2n) for Al (a), Na (b), and F (c) isotopes calculated using various Skyrme parameterizations within SHF and compared with experimental data taken from Ref. [22]

4.3.3. Shell evaluation

Fig. 6. describes the energy of the neutron single particle state in Al(a), Na(b), and F(c) isotopes. For this purpose, we used the parameters skxcsb, skxsdd, skxta, skxtb, and sly4. The parameters skxtb and skxcsbb reflect the significant impact of the island of inversion on the state distribution. For the parameter skxtb, it can be observed, specifically in Fig. 6(a), that there is a convergence between two states, $1f_{5/2}$ and $1p_{1/2}$, to the point that there is a disappearance of the natural gap between them in the natural distribution of the Shell Model. This convergence is due to the tensor force, In Figs. 6 (b) and 6 (c), the distribution of states is the same. The tensor force also contributes to the convergence between $1p_{3/2}$ and $1p_{1/2}$ states. Regarding the parameter skxcsbb, we observe the emergence of intruder states that occupy the positions of other states. For

International Journal of Environmental Sciences
ISSN: 2229-7359
Vol. 11 No. 12s,2025
https://theaspd.com/index.php

instance, we find state $2f_{7/2}$ above state $2p_{3/2}$ as an intruder state. This is one of the most significant features of the island inversion.

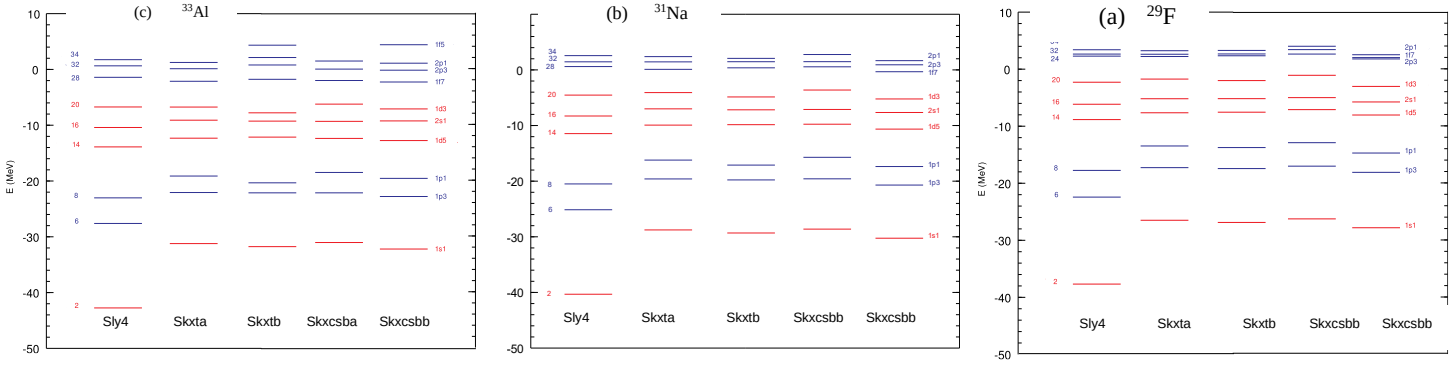

Fig. 6 (a),(b), and (c). Neutron single-particle energy levels for ^{33}Al,^{31}Na, and ^{29}F using shell model with different Skyrme parameterizations as a single-particle potential.

4.3.4. Longitudinal electroexcitation form factors

The left panel of Fig. 7. illustrates the longitudinal form factors C2 for Al, Na, and F isotopes. We compute the C2 form factors by incorporating effective charges to account for the consequences of model-space truncation. The sd model space is employed to conduct microscopic calculations of the effective charges for the aforementioned nuclei. We compared the experimental results for the changes ($J^{\pi}=0^{+}\rightarrow J^{\pi}=2^{+}$) to the calculated results for the inelastic longitudinal form factors of all the nuclei we are studying. These are plotted against the momentum transfer q. Although they have the same proton number, it is evident that the form factors of each isotope are significantly distinct from those of other isotopes. The curve exhibits a shift in the minima position compared to others. The reason for this alteration is the differences in the center of mass correction, which are contingent upon the size parameter and the mass number. The longitudinal form factor for the nuclei under study at high momentum transfer is depicted in the right panel of Fig. 7. The interference effects between dispersed waves become more pronounced as the form factor becomes more sensitive to the detailed structure of the scattering. This can lead to oscillatory or non-uniform behavior in the form factor curve. Al-33, Na-31, and F-29 are nuclei that are situated on the island of inversion and possess distinctive nuclear structure characteristics. Unanticipated behaviors in form factors and other nuclear properties may result from the disruption of the normal ordering of energy levels on the island of inversion. The intruder state in configurations and other structural features associated with nuclei on the island of inversion are the causes of the deviation from the expected normal curve.

International Journal of Environmental Sciences
ISSN: 2229-7359
Vol. 11 No. 12s,2025
https://theaspd.com/index.php

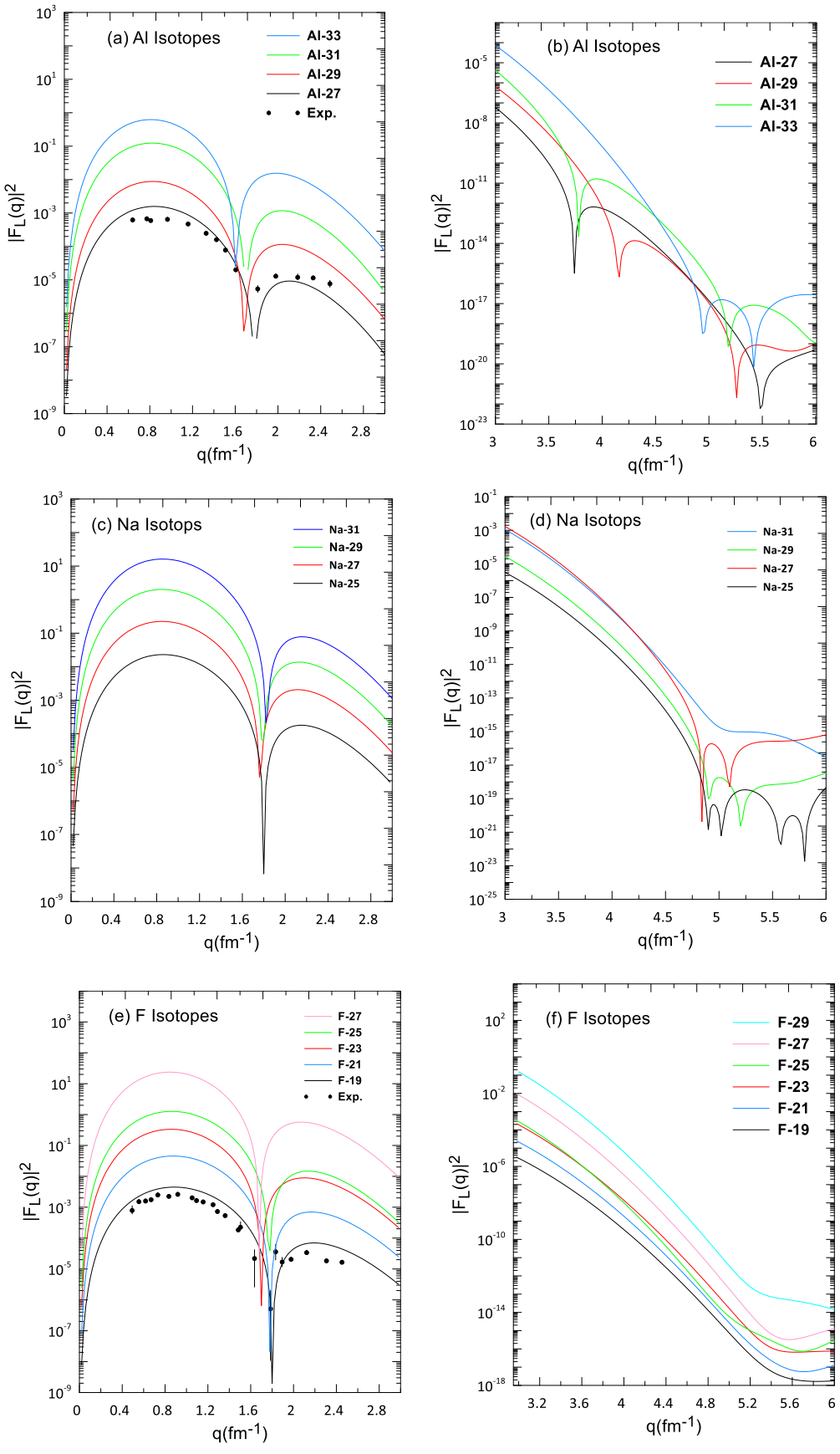

Fig. 7. Theoretical longitudinal form factor C2 for low and high momentum transfer form for Al, Na and F isotopes compared with the experimental data taken from Ref. [23,24]

4. CONCLUSIONS

We investigate the static and dynamic nuclear structure properties of Al, Na, and F isotopes through a combination of large-scale shell model calculations. Shell model calculations were performed in the sd-shell model space using the USDA, USDB, and USDC effective interactions, and in a truncated no-core *spsdpf* model space using the FSU interaction. The results demonstrate that while traditional sd-shell interactions are inadequate for capturing the enhanced collectivity and cross-shell excitations characteristic of the island of inversion, the FSU interaction provide a much-improved description of the evolving shell structure.

References

1-A. A. Alzubadi, N. F. Latooffi, and R. A. Radhi, Int. J. Mod. Phys. E 24, 1550099 (2015).
2- R. A. Radhi and A. A. Alzubadi, Few-Body Syst. 60, 57 (2019).
3- O. Sorlin and M.-G. Porquet, Prog. Part. Nucl. Phys. 61, 602 (2008).
4- L. J. Abbas and A. A. Alzubadi, Iraqi J. Phys. 19, 89 (2021).
5- B. A. Brown, Prog. Part. Nucl. Phys. 47, 517 (2001).
6- B. A. Brown and W. A. Richter, Phys. Rev. C 74, 034315 (2006).
7- N. A. Smirnova et al., Phys. Rev. C 100, 054329 (2019).
8- R. S. Lubna et al., Phys. Rev. Res. 2, 043342 (2020).
9- R.A. Radhi et al., Nuc. Phys. A 1015 (2021)122302
10- V. Tripathi et al., Phys. Rev. Lett. 94, 162501 (2005).
11- P. Doornenbal et al., Phys. Rev. C 81, 041305 (2010).
12- E. Caurier, F. Nowacki, and A. Poves, Phys. Rev. C 90, 014302 (2014).
13- B. A. Brown and W. D. M. Rae, Nucl. Data Sheets 120, 115 (2014).
14- P. Ring and P. Schuck, *The Nuclear Many-Body Problem*, 3rd edn., Springer, New York (2004).
15- D. Vautherin and D. M. Brink, Phys. Rev. C 5, 626 (1972).
16- E. Suckling, MSc Thesis, *Study of Magic Number Evolution in Exotic Nuclei*, University of Surrey (2006).
17- H. Sagawa, B. A. Brown, and O. Scholten, Phys. Lett. B 159, 228 (1985).
18- T. De Forest and J. D. Walecka, Adv. Phys. 15, 1 (1966).
19- A. Bohr and B. R. Mottelson, *Nuclear Structure*, Vol. I, World Scientific, Singapore (1988).
20- B. A. Brown, R. A. Radhi, and B. H. Wildenthal, Phys. Rep. 101, 313 (1983).
21- T. Sil, S. K. Patra, B. K. Sharma, M. Centelles, and X. Viñas, Phys. Rev. C 69, 044315 (2004).
22- National Nuclear Data Center (NNDC), https://www.nndc.bnl.gov/
23- P. J. Ryan, J. Rapaport, C. D. Goodman, and T. N. Taddeucci, Phys. Rev. C 27, 2515 (1983).
24- B. A. Brown, B. H. Wildenthal, M. S. Antony, and A. H. Wapstra, Phys. Rev. C 32, 1127 (1985).